

Experimental determination of the buckling load of rectangular plates using vibration correlation technique

Paired Singhatanadgid* and Padol Sukajit

*Department of Mechanical Engineering, Faculty of Engineering, Chulalongkorn University,
Bangkok, 10330, Thailand*

(Received September 23, 2009, Accepted October 14, 2010)

Abstract. This study investigates the use of a vibration correlation technique (VCT) to identify the buckling load of a rectangular thin plate. It is proposed that the buckling load can be determined experimentally using the natural frequencies of plates under tensile loading. A set of rectangular plates was tested for natural frequencies using an impact test method. Aluminum and stainless steel specimens with CCCC, CCCF and CFCF boundary conditions were included in the experiment. The measured buckling load was determined from the plot of the square of a measured natural frequency versus an in-plane load. The buckling loads from the measured vibration data match the numerical solutions very well. For specimens with well-defined boundary conditions, the average percentage difference between buckling loads from VCT and numerical solutions is -0.18% with a standard deviation of 5.05% . The proposed technique using vibration data in the tensile loading region has proven to be an accurate and reliable method which might be used to identify the buckling load of plates. Unlike other static methods, this correlation approach does not require drawing lines in the pre-buckling and post-buckling regions; thus, bias in data interpretation is avoided.

Keywords: buckling load; vibration; natural frequency; thin plate; experiment.

1. Introduction

Buckling load is one of the important parameters which should be considered in the design of thin or slender structures subjected to compressive loading. The buckling behavior of engineering structures such as columns, plates, frames, and shells has been continuously investigated in the past several decades. Thin plates are among the most important of the many types of structures used in engineering applications.

The stability problem of a plate can be investigated using theoretical, numerical and experimental approaches. The theoretical method is applicable to a limited type of problem, where a closed-form solution is possible. For more complicated structures, numerical methods such as a finite element method are required. Solutions from both theoretical and numerical methods are generally verified with experimental results. Experimental methods involve a number of costly and time-consuming processes; however, imperfections and complications are naturally included in any scientific inquiry.

*Corresponding author, Ph.D., E-mail: Paired.S@chula.ac.th

In an experimental study of plate buckling, identification of the buckling point is an important part of the process, since it directly affects the accuracy of the measurement. In the experiment, the buckling load of plates can be identified using various kinds of plots; for example: 1) a plot of in-plane loads vs. out-of-plane displacement; 2) a plot of in-plane loads vs. end-shortening; and 3) a plot of in-plane loads vs. difference of surface strains. These methods, which may be classified as static methods, utilize the change of the slope of the curve in pre-buckling and post-buckling regions to identify buckling load. The plots mentioned above, as well as other static methods, are summarized by Singer *et al.* (1992).

Several studies have employed static methods to identify the buckling load of plates. Chai *et al.* (1991) verified the theoretical buckling load of composite plates using an experimental method. Buckling load was determined from the intersection of the tangents drawn in the pre-buckling and post-buckling slopes of the load versus membrane strain curve. Discrepancies between the experimental and theoretical solutions of between -7% and $+11\%$ were reported. Tuttle *et al.* (1999) determined buckling loads of composite panels from the plots of applied in-plane load vs. out-of-plane displacement, and compared the experimental results to numerical predictions obtained using a Galerkin method. Although the average percentage error between the measured and predicted buckling loads is low, the standard deviation of the percentage error is as high as 15% . The difficulties of identifying the buckling load using a static test method were documented. In particular, drawing two lines in the pre-buckling and post-buckling regions to identify the buckling point depended on personal judgment, and could be a cause of error. To use the experimental result as a benchmark solution, the method used to identify buckling load must be accurate and reliable.

There is a need for an alternative approach to experimentally identify the buckling load of a plate. In this paper, vibration correlation technique (VCT) is explored and modified to determine the buckling load of a plate. VCT is a nondestructive test utilizing measured vibration data. This concept has been applied to buckling problems in the past, with a varying amount of success. Lurie and Monica (1952) showed that the square of the frequency of the lateral vibration of a thin plate with simple supports on all edges is linearly related to the end load. They also conducted some experiments on elastically restrained columns, rigid-joint trusses, and thin flat plates. The authors reported that VCT was successfully employed to predict the buckling load of only columns and trusses. For flat plates, because of the initial curvature, the buckling load cannot be predicted by the proposed method. However, Chailleux *et al.* (1975) later showed that with a carefully designed experimental setting, VCT can be used to determine the buckling load with satisfactory accuracy. The experimental dynamic curve is linear in the low-load region, so it is possible to extrapolate the data to obtain the buckling load. Segall and Springer (1986) proposed a dynamic method to determine linear buckling loads of elastic rectangular plates. With an integral equation representation of the elastic stability, their proposed technique does not require the application of an in-plane load. A few studies (Souza and Assaid 1991, Go *et al.* 1997, Go and Liou 2000) including a report by Singhatanadgid and Sukajit (2008) which is the pilot investigation of this study, concerning the use of vibration data to investigate buckling behavior can be found in the literature.

In this study, the relationship between buckling and vibration behavior of thin plates is investigated. The relationship between applied in-plane load and the natural frequency of plates is derived from the governing differential equations of both problems. The derived relationship, which is applicable to thin plates with any boundary conditions, is numerically verified by simulating a plot of the derived relationship. Because of the premature curvature, which is usually detected even before the specimen has buckled, it is proposed in this study that the buckling load be determined

from the vibration data of a plate subjected to tensile loading. A test frame, capable of applying tensile and compressive loading to a specimen, was prepared. A series of vibration tests was performed to determine the natural frequencies of the plates. The vibration data, along with the derived relationship, were used to predict the buckling load. Experimental buckling loads were compared to the numerical solutions to verify the proposed technique.

2. Relationship between natural frequency and buckling load

The vibration correlation technique utilizes the relationship between vibration parameters and buckling parameters. If the relationship between both parameters is established, the buckling behavior can be determined from the known or measured vibration parameters. In this section, vibration and buckling behaviors of a thin plate are investigated and their relationship is derived. As shown in Fig. 1, a rectangular plate with a dimension of $a \times b$ and subjected to a uniform uniaxial loading N_x is a system of interest. For a buckling problem, an applied in-plane load N_x is always a compressive load. The desired parameters to be determined are buckling load and buckling mode. The buckling load of a plate – represented by \bar{N}_x – is the in-plane compressive load N_x at which buckling occurs, while the buckling mode is the out-of-plane configuration w of the buckled plate. In addition, natural frequencies and vibration mode shapes are two parameters to be determined in a vibration problem. The natural frequencies of a plate can be determined for a specimen with a given N_x . It should be noted that \bar{N}_x and N_x refer to the same in-plane load; however, \bar{N}_x is the buckling load, which must be a compressive load (negative value); while N_x is the applied in-plane load, which can be either tension or compression. To derive the relationship between both phenomena, the governing equations of both problems are considered. The governing equations for buckling and vibration of a thin isotropic plate are written as

$$\frac{\partial^4 w}{\partial x^4} + 2 \frac{\partial^4 w}{\partial x^2 \partial y^2} + \frac{\partial^4 w}{\partial y^4} - \frac{\bar{N}_x}{D} \frac{\partial^2 w}{\partial x^2} = 0 \tag{1}$$

and

$$\frac{\partial^4 w}{\partial x^4} + 2 \frac{\partial^4 w}{\partial x^2 \partial y^2} + \frac{\partial^4 w}{\partial y^4} - \frac{N_x}{D} \frac{\partial^2 w}{\partial x^2} - \frac{\omega^{*2} \rho}{D} w = 0 \tag{2}$$

respectively. D is the flexural rigidity and is defined by

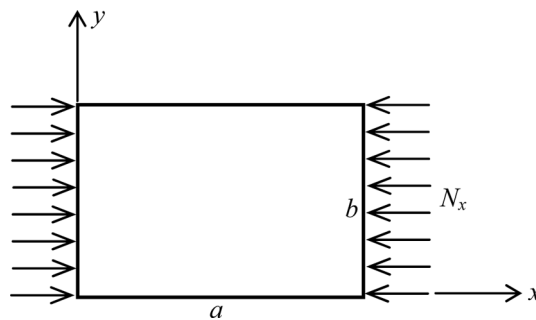


Fig. 1 A rectangular plate subjected to a uniaxial in-plane load N_x

$$D = \frac{Eh^3}{12(1-\nu^2)}$$

E is Young's modulus, h is the plate thickness and ν is Poisson's ratio. For a given plate with particular boundary conditions, it is widely known that the buckling mode is identical to one of the vibration modes. Specifically, the out-of-plane displacement of the buckled plate is the same as the out-of-plane displacement of one of the vibration modes. So, the governing equation of the buckling problem can be rewritten as

$$L_1(w) - \bar{N}_x L_2(w) = 0 \quad (3)$$

where $L_1(w) = \frac{\partial^4 w}{\partial x^4} + 2\frac{\partial^4 w}{\partial x^2 \partial y^2} + \frac{\partial^4 w}{\partial y^4}$ and $L_2(w) = \frac{1}{D} \frac{\partial^2 w}{\partial x^2}$.

Similarly, the governing equation of the vibration of loaded plates is written as

$$L_1(w) - N_x L_2(w) - \omega^{*2} L_3(w) = 0 \quad (4)$$

where $L_3(w) = \rho w/D$.

It should be noted that the terms containing derivatives of w are the same for both problems because the buckling mode and vibration mode are identical. From Eq. (3), the buckling load of a plate can be written as

$$\bar{N}_x = \frac{L_1(w)}{L_2(w)} \quad (5)$$

Similarly, the natural frequency of a plate, with the applied in-plane load N_x , can be determined from Eq. (4), and written as

$$\omega^{*2} = \frac{L_1(w) - N_x L_2(w)}{L_3(w)} \quad (6)$$

where ω^* is the natural frequency of a plate with applied load N_x . It is noticed that the natural frequency of a plate varies with the in-plane loading. For an unloaded plate, the natural frequency is simply described as

$$\omega^2 = \frac{L_1(w)}{L_3(w)} \quad (7)$$

where ω is the natural frequency of a plate without an applied load. By dividing Eq. (5) by Eq. (6) and utilizing Eq. (7), the ratio of the square of the natural frequency of a loaded plate to that of an unloaded plate is written as

$$\left(\frac{\omega^*}{\omega}\right)^2 = 1 - \frac{N_x}{\bar{N}_x} \quad (8)$$

From the relationship shown in Eq. (8), both the buckling load \bar{N}_x and the natural frequency of an unloaded plate ω may be considered as a constant for a specific specimen. The variables in that equation are the natural frequency of the loaded plate ω^* and the applied in-plane load N_x . Thus, the square of the natural frequency (ω^{*2}) varies linearly with the applied load N_x . With the buckling load being a negative value, it is observed that the natural frequency of the plate increases with the applied tensile load. On the other hand, it decreases with the applied compression.

Moreover, if the applied load N_x equals the buckling load of the plate, the natural frequency ω^* theoretically equals zero. Based on this observation, the natural frequencies of the loaded plate can be utilized to predict its buckling load by plotting ω^{*2} versus the in-plane load N_x . The buckling load can be determined from the applied load N_x at which the natural frequency approaches zero. Since this relationship is derived from the governing equations, it is applicable to specimens with any boundary conditions. In addition to conventional boundary conditions, this relationship is also applicable for thin plates with unknown or imperfect boundary conditions. As long as the vibration data is obtained from a given specimen with specific boundary conditions, the buckling load determined using VCT will be the buckling load of that specimen.

Numerical verification

To numerically verify the VCT and the derived relationship shown in Eq. (8), a numerical simulation of the vibration and buckling of a plate was performed. The Ritz method with characteristic beam functions was used to solve the buckling and vibration problems. Detailed information about the Ritz method, which is beyond the scope of this paper, can be found in Ding (1996), Rajalingham *et al.* (1996), Lee *et al.* (1997), Aydogdu *et al.* (2003), Wang *et al.* (2005), Timarci *et al.* (2005) and Ni *et al.* (2005). A 2-mm-thick aluminum plate with a dimension $a \times b$ of 400x200 mm² was chosen as a specimen. The plate was assumed to be simply supported on the loading edges and clamp-supported on the other two edges. The buckling load of this specimen was numerically determined, and found to be 88.216 kN/m with buckling mode (3, 1). The buckling mode of this specimen is graphically shown in Fig. 2. The numerical solution serves as the theoretical solution for this simulation, and is used to validate the buckling load from VCT. Buckling load and mode determined from VCT requires the vibration data, i.e., natural frequencies and vibration mode shapes, of the plate subjected to in-plane loading. These vibration parameters of the loaded plated were also simulated using the Ritz method. The applied in-plane load was increased step by step in both tensile and compressive loading ranges. The square of the natural frequencies for the first six modes was plotted versus applied load, as shown in Fig. 3. The mode shape of each vibration mode is shown in Fig. 4. The relationship between ω^{*2} and N_x of a particular vibration mode is linear, as expected according to the derived relationship. The predicted buckling load can be determined by extrapolating the vibration data to the in-plane load at which the square of the natural frequency approaches zero. Trend lines of each vibration mode intercept the N_x axis at a different load level. The lowest compressive load is the buckling load, and its corresponding vibration mode shape is the predicted buckling mode. In this simulation, the predicted buckling is 88.216 kN/m and the buckling mode is mode (3, 1). VCT predicted the

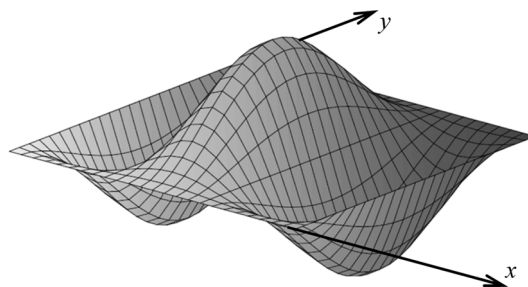


Fig. 2 Buckling mode determined from the buckling problem

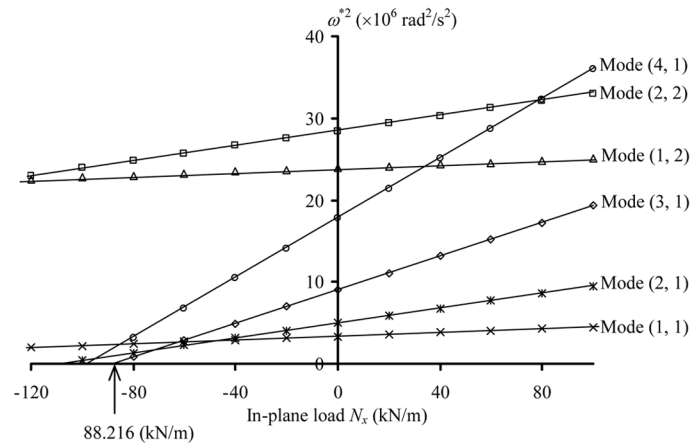


Fig. 3 Square of the natural frequencies of an aluminum plate vs. applied loading

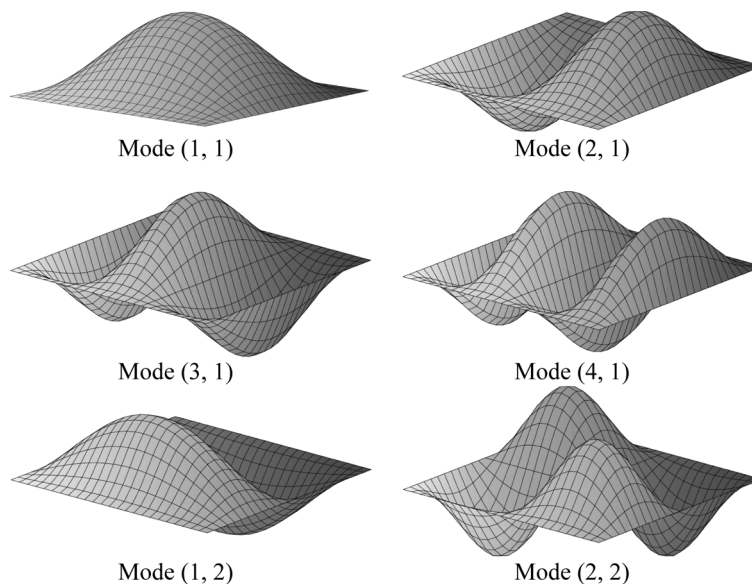


Fig. 4 Vibration mode shapes of the first six vibration modes

buckling mode to be mode (3, 1) because the trend line of this vibration mode intersects the N_x axis at the lowest load, compared to those of other vibration modes. The buckling load determined from the vibration data compares perfectly with the numerical solution. Similarly, the buckling mode determined from VCT is also identical to the buckling mode of the numerical solution. In conclusion, the squares of the natural frequencies vary linearly with the applied in-plane load, as expected from the relationship shown in Eq. (8). The natural frequency approaches zero as the in-plane compressive load approaches the buckling load of plate. The numerical simulation showed that buckling behaviors of a thin plate can be accurately predicted using VCT. The concept of using vibration parameters to identify buckling load and mode is thus theoretically verified. However, further experimental study is required to determine the accuracy and reliability of the technique.

3. Experimental arrangement

Although the relationship between vibration and buckling behaviors of a thin plate is theoretically confirmed, the applicability of VCT as an experimental technique which can be used to identify buckling load requires further investigation. A series of experiments was performed to determine the accuracy and reliability of the proposed technique. A set of aluminum and stainless steel plates was used; each plate was uniaxially loaded on a custom-made test frame. The experiment was then performed on the loaded specimens to determine natural frequencies and vibration mode shape. The vibration data was obtained for the specimens subjected to both tensile and compressive loading. The measured natural frequencies and applied loading were then plotted, with results similar to those shown in Fig. 3. The predicted buckling load was identified using VCT, i.e., the relationship derived previously.

3.1 Test frame

The test setup, shown in Fig. 5, was specifically designed to accommodate the loading configurations and vibration testing. The test frame is capable of applying both clamped and free boundary conditions to the specimens (The simple supported boundary condition was not included in the experiment because it is difficult to obtain a perfect simple support compared with the other two conventional boundary conditions). Both tensile and compressive loads can be applied on the specimens. In-plane loads are applied horizontally using a hydraulic cylinder pressurized with a hand pump. The hydraulic cylinder is mounted on the right end frame, which is fixed to the left end frame using two guided columns. A rectangular thin plate is mounted on the loading edges, with clamped support between crosshead #2 and crosshead #3.

For a tensile testing configuration, as shown in Fig. 5, the hydraulic ram applies a compressive

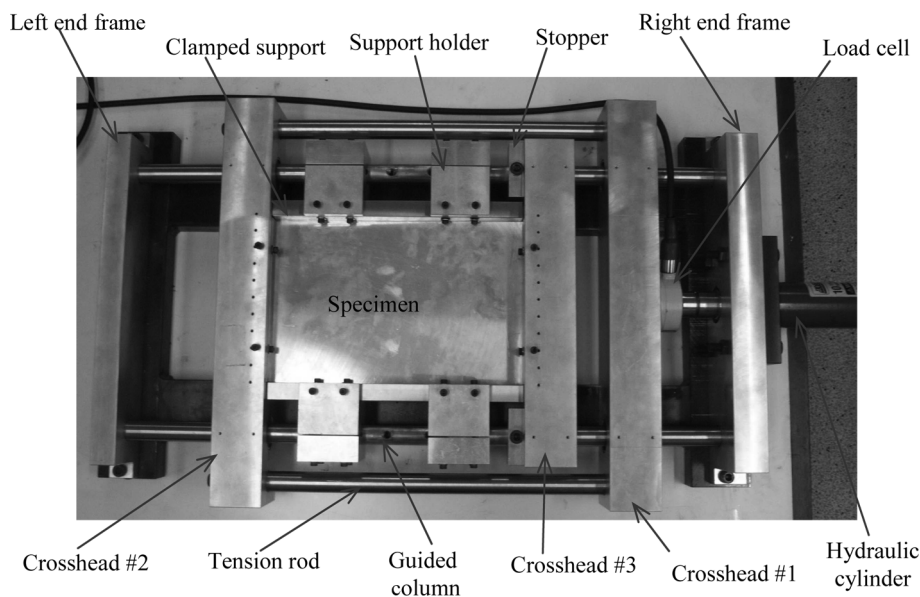


Fig. 5 Experimental setup of a specimen with CCCC boundary condition subjected to tensile loading

force against crosshead #1. Loads are monitored using a load cell mounted between crosshead #1 and the hydraulic cylinder. Two linear bearings are embedded within the crossheads so they can move linearly along two guided columns. The applied loading on crosshead #1 is transferred through two tension rods to crosshead #2. Crosshead #2 thus is pushed, and tends to move to the left-hand side. On the other hand, crosshead #3 is blocked by two stoppers mounted on the guided columns, as shown in the figure. With this loading configuration, a specimen which is clamped between crosshead #2 and crosshead #3 is stretched when the compressive load is applied by the hydraulic ram.

In the case of compressive testing, the test frame shown in Fig. 5 must be modified. Crosshead #1 and the tension rods are removed in the compressive testing configuration. The two stoppers which are used to block crosshead #3 in the tensile testing configuration are moved to the left-hand side of crosshead #2, to prevent the horizontal motion of the crosshead. A compressive load from the hydraulic ram is then applied directly on crosshead #3. With this setup, the specimen is uniformly compressed between crosshead #2 and crosshead #3. Hence the designed test frame is capable of applying both tensile and compressive loads to a thin plate with changeable loading configurations.

Besides the loading mechanism, the test frame is also equipped with restraining devices to apply desired boundary conditions to the test samples. In Fig. 5, the clamped boundary conditions of the specimen are enforced by 20-mm-thick rigid stainless steel bars, denoted as “clamped support.” For the unloaded edges, the clamped supports are mounted on the support holders, which are tightly clamped to the guided columns. Similarly, the rigid stainless steel bars are placed in the slots of the crossheads to assemble a clamped support on the loaded edges. On both loaded and unloaded edges, machine screws are used to push the steel supports against the specimen surface. To obtain a clamped support, machine screws are finger-tightened until the gap between the specimen and support is invisible. Clamped supports on the unloaded edges of the specimen can be removed so that a free edge is formed on those boundaries. With the described constraint mechanism, the boundary conditions of a specimen consist of clamped support on the loaded edges ($x = 0$ and $x = a$), and either clamped or free edges on the unloaded edges ($y = 0$ and $y = b$).

3.2 Test specimens

A series of experiments was performed on 12 thin isotropic plates with CCCC, CCCF and CFCF boundary conditions. The symbol “C” represents a clamped boundary condition, while “F” stands for a free boundary condition. The first and third letters symbolize the boundary conditions on $x = 0$ and $x = a$, respectively. Similarly, the boundary conditions on $y = 0$ and $y = b$ are represented by the second and fourth letters, respectively. The specimens were prepared from 6061-T6 aluminum alloy and stainless steel AISI 304. The physical and mechanical properties of both materials are presented in Table 1. Nominal dimensions $a \times b$ of the specimens were 300×200 , 200×200 , and 150×200 mm². For each plate size, there were two specimens with different thicknesses. Thus, there were a

Table 1 Properties of materials used in the experiments

Material	Modulus of Elasticity, E (GPa)	Poisson ratio, ν	Density, ρ (kg/m ³)
Aluminum 6061-T6	70	0.33	2700
Stainless steel AISI 304	193	0.30	8000

Table 2 Buckling load in kN/m of aluminum specimens compared to numerical solutions

Specimen No.	Dimension ($a \times b$) mm ²	Thickness, mm	CCCC			CCCF			CFCF			
			Numerical Solution	Exp. Measurement	% Diff	Numerical Solution	Exp. Measurement	% Diff	Numerical Solution	Exp. Measurement	% Diff	
1	300 × 200	2.032	113.2	115.7	2.21	34.0	34.8	2.43	23.5	24.1	2.40	
2	300 × 200	2.298	163.7	165.6	1.14	49.2	46.6	-5.35	34.0	34.2	0.48	
3	200 × 200	1.765	89.5	89.0	-0.53	40.7	38.3	-5.95	34.9	33.7	-3.43	
4	200 × 200	1.955	121.6	125.1	2.90	55.3	54.8	-0.90	47.4	46.8	-1.39	
5	150 × 200	1.745	100.1	101.1	0.94	65.5	64.8	-1.01	60.2	57.1	-5.18	
6	150 × 200	1.976	145.4	146.5	0.75	95.1	99.0	4.10	87.4	84.5	-3.28	
Average					1.24				-1.11			
Standard deviation					4.44				6.30			

Table 3 Buckling load in kN/m of stainless steel specimens compared to numerical solutions

Specimen No.	Dimension ($a \times b$) mm ²	Thickness, mm	CCCC			CCCF			CFCF			
			Numerical Solution	Exp. Measurement	% Diff	Numerical Solution	Exp. Measurement	% Diff	Numerical Solution	Exp. Measurement	% Diff	
1	300 x 200	1.173	58.8	62.5	6.35	18.0	19.0	5.13	12.3	12.0	-1.87	
2	300 x 200	1.389	97.6	112.6	15.38	29.7	28.4	-4.21	20.4	20.6	0.87	
3	200 x 200	1.110	60.1	64.6	7.58	27.5	28.4	3.18	23.5	23.6	0.48	
4	200 x 200	1.389	117.7	133.6	13.45	53.9	55.2	2.33	46.1	46.7	1.32	
5	150 x 200	1.124	72.3	79.2	9.55	47.4	48.3	1.91	43.5	44.2	1.43	
6	150 x 200	1.406	141.4	164.3	16.15	92.8	87.3	-5.91	85.2	N/A	N/A	
Average					11.41				0.40			
Standard deviation					6.23				5.95			

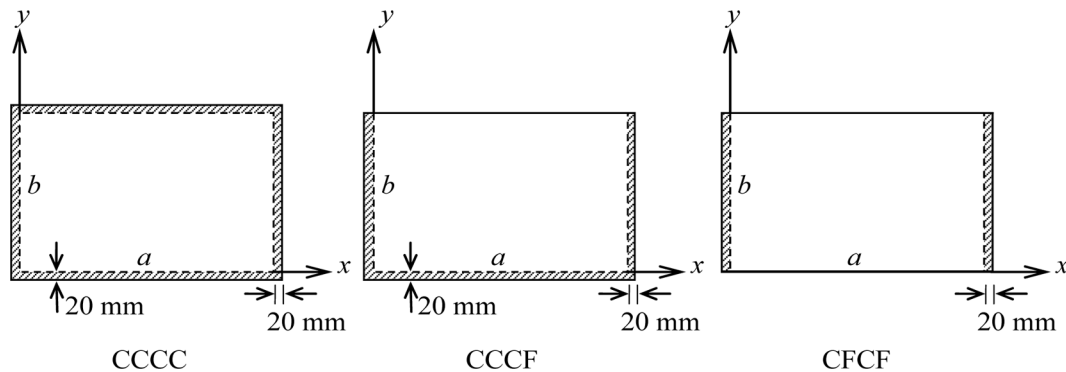


Fig. 6 Nominal and actual dimensions of the specimens

total of six aluminum specimens and six stainless steel specimens. The aluminum and stainless steel specimens' dimensions are summarized in the first three columns of Table 2 and Table 3, respectively. It should be noted that the actual size of a specimen is slightly larger than the nominal size because a small portion on the boundary of the specimen is clamped by the rigid stainless steel bar, and is not regarded as an effective area. The schematic dimensions of the specimens are presented in Fig. 6.

Each specimen was originally prepared to be a CCCC specimen. The width and height of all specimens were 40 mm larger than those of the nominal dimensions. A 20-mm-wide area on each of the four edges was reserved as an area to be clamped by a support. In the schematic of a CCCC specimen shown in Fig. 6, the effective area or nominal area of the specimen is represented by a clear area of $a \times b$, whereas the dashed area is an area to be clamped by the support. After an experiment on a CCCC specimen was concluded, a clamped area on one of the unloaded edges was cut off to form a CCCF specimen. So, the actual size of a CCCF specimen was slightly smaller than a CCCC specimen with the same nominal size. Finally, the other clamped area on the unloaded edges was removed to obtain a CFCF specimen. Thus, specimens with an equal nominal size but different boundary conditions are actually the same specimen.

3.3 Testing procedures

In this study, the natural frequencies of a loaded plate are required data in order to predict the buckling behavior of the plate. Vibration testing was performed using an impact test, in which the specimen was excited by an impact hammer while the applied impulse was monitored by a dynamic signal analyzer. Acceleration response of the specimen was measured by an accelerometer placed on the specimen at a selected location. Acceleration data measured in the time domain were processed by a fast Fourier transform algorithm using the dynamic signal analyzer to obtain the frequency response function (FRF). From the vibration response in the frequency domain, the natural frequencies of the specimen were identified from the peak of the response. Vibration mode shape was also obtained from an imaginary part of the response function. An overview of the vibration testing and modal analysis is beyond the scope of this paper; the interested reader is referred to the article by Avitabile (2001). The typical magnitude and imaginary part of the frequency response function are shown in Fig. 7.

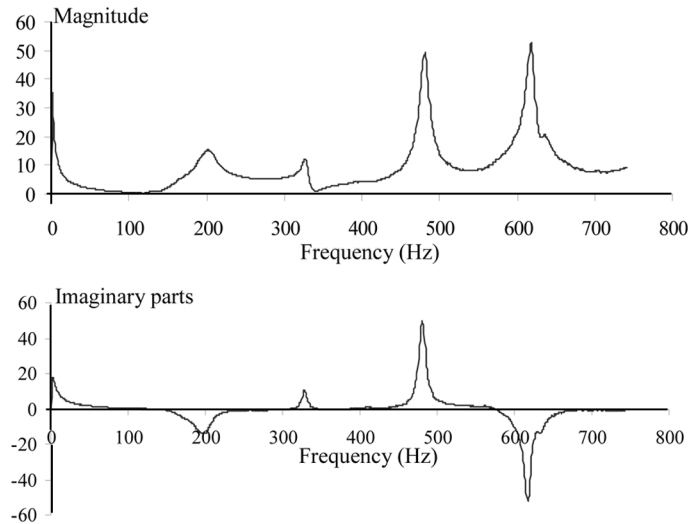


Fig. 7 Magnitude and imaginary parts of the frequency response of CCCC stainless steel specimen #2, without an in-plane load

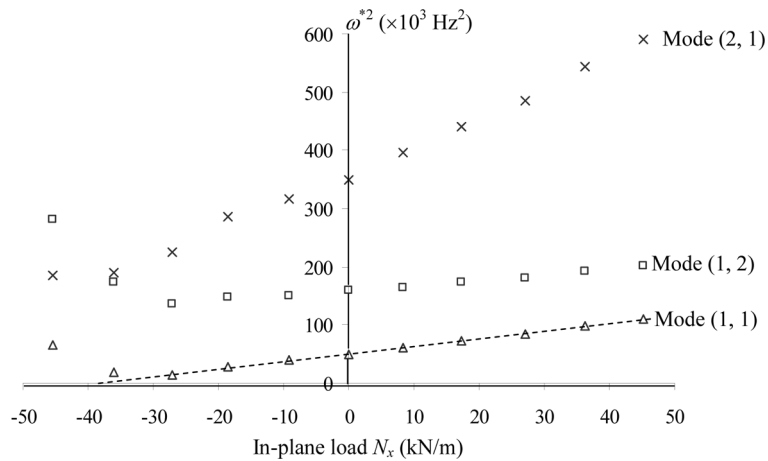


Fig. 8 Plot of ω^2 vs. N_x of aluminum specimen #3, with CCCF boundary condition

The experiment on a specimen was composed of two parts. The first part of the experiment was performed to verify the relationship shown in Eq. (8) and to determine the buckling mode of the plate. The specimen was loaded in both tensile and compressive loading ranges. Natural frequencies of the specimen under unloaded, tensile-loaded and compressive-loaded conditions were determined, respectively. The square of the natural frequency was plotted against applied in-plane load. A typical relationship between ω^2 and N_x is presented in Fig. 8, which is the vibration behavior of aluminum specimen #3 with CCCF boundary condition. Natural frequencies of vibration modes (1, 1), (1, 2) and (2, 1) are included in the plot. Numbers representing a vibration mode stand for the number of curves of an out-of-plane displacement in the x and y directions, respectively. Vibration mode shape is determined from the imaginary parts of the frequency response from several

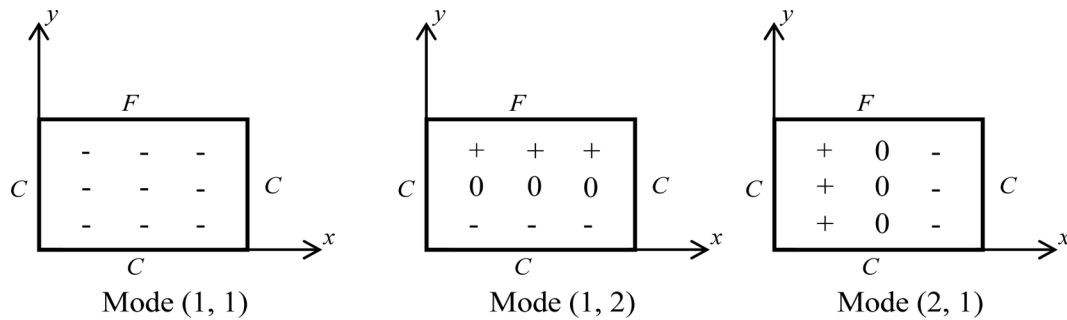


Fig. 9 Vibration mode shapes of the experiments shown in Fig. 8

experiments. A plot of each mode shape is presented in Fig. 9. The symbols “-” and “+” represent the out-of-plane displacement in different directions on the specimens, and “0” indicates a zero displacement or a node line. From the results shown in Fig. 8, the buckling mode of the specimen was determined to be mode (1, 1), since the trend line of this mode intersects the N_x axis at the lowest value. It is observed that ω^{*2} varies linearly with the applied load in the tensile loading range, as expected. The relationship between both parameters in the compressive loading range is not as linear as the relationship in the tensile loading range. This nonlinear relationship in the compressive loading range was also observed in other specimens, and was previously reported by Lurie and Monica (1952). This behavior is contradicted by the result from the numerical simulation shown in Fig. 3. It is speculated that the nonlinear behavior is a result of a premature curvature which develops before buckling of the specimen. For this reason, the buckling load was determined using only vibration data of the specimen subjected to tensile loading.

The second part of the experiment focused on determining the buckling load. After plotting the relationship of ω^{*2} vs. N_x , as previously seen in Fig. 8, and determining the buckling mode, the specimen was reloaded under increased levels of tensile loading. At each load level, a vibration test was performed to determine the natural frequency of the loaded plate. Only the natural frequencies of the relevant mode shape, i.e., the buckling mode, were collected. A plot of ω^{*2} versus N_x in the tensile loading range was generated and extrapolated to determine the measured buckling load. Because the measurement of natural frequency is very sensitive to boundary conditions, the experiment was repeated 20 times by loosening and re-tightening the machine screws on the clamped supports. An average of the measured buckling load is reported as the buckling load obtained from VCT.

4. Experimental results and discussion

All 12 specimens were tested to determine natural frequencies for each vibration mode. For each vibration mode, the square of the natural frequency was plotted against an applied load to determine buckling load and buckling mode.

4.1 Buckling mode

The experimental buckling mode is determined from the vibration mode whose trend line

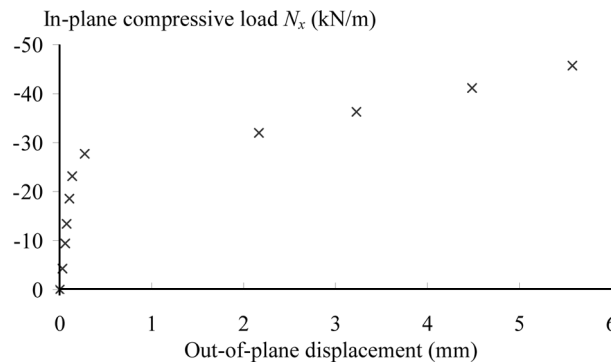


Fig. 10 Plot of applied load vs. out-of-plane displacement of the specimen shown in Fig. 8

intersects the N_x -axis at the lowest load level. For all specimens, buckling modes determined from the experiment correspond very well to the numerical solutions. The plots of ω^{*2} vs. N_x for all specimens are similar to that of aluminum specimen #3, which is shown in Fig. 8. The relationship between both parameters is linear throughout both the tensile loading range and the low-load compressive loading range. In the high-load range, most of the experimental results showed that the squares of the natural frequencies do not vary linearly with the in-plane loads. In Fig. 8, nonlinear behavior is observed when the applied compressive load is greater than approximately 30 kN/m. To investigate the cause of this nonlinear behavior, the maximum out-of-plane displacement of the specimen subjected to compressive loading was measured and plotted, as shown in Fig. 10. From the figure, it is apparent that the out-of-plane displacement is observed as soon as the compressive load is applied. In the low-load range, i.e., N_x lower than 25 kN/m, the measured out-of-plane displacement is less than 0.3 mm. The out-of-plane displacement is more pronounced as the applied load approaches 30 kN/m. From linear buckling theory, the out-of-plane displacement cannot exist before the specimen has buckled. So this out-of-plane displacement could be considered to be a premature deformation in the experiment, reflecting imperfections in either the specimen or the test setup. The in-plane compressive load level at which the square of the natural frequency begins to be nonlinear corresponds very well with the load level where the out-of-plane displacement of the specimen is well-defined. Other specimens also exhibited a similar correlation between the load level where a distinct out-of-plane displacement is observed, and the load level where a nonlinear behavior between ω^{*2} and N_x is observed. It is reasonable to draw the conclusion that ω^{*2} does not vary linearly with the in-plane load in the high compressive loading region because of the premature out-of-plane displacement developed there. Therefore, the proposal to use vibration data in the tensile loading range to identify buckling load is justified.

4.2 Buckling load

The buckling loads determined from VCT for aluminum and stainless steel specimens are compared with numerical solutions in Tables 2 and 3, respectively. The experimental buckling load is determined from a plot of vibration data in the tensile loading range. In Tables 2 and 3, dimensions of the specimens are presented in the first three columns. The next three columns compare experimental buckling loads of CCCC specimens with numerical solutions which are used as benchmarks. The last six columns show the experimental results of CCCF and CFCF specimens.

(It should be noted that the experimental CFCF result of stainless steel specimen #6 is inapplicable, because the specimen was permanently bent during the compressive test.) Each experimental buckling load presented in Tables 2 and 3 is an average value based on a set of 20 experiments. The discrepancy between the experimental buckling load and the benchmark solution is presented as a percentage difference, as shown in the columns denoted by “% Diff.” Average and standard deviations of the percent difference between experimental and numerical solutions of specimens with the same boundary conditions are shown at the bottom of the tables. Since the experimental buckling loads are an average value from 20 experiments, standard deviations shown in the last row are calculated from 120 experiments for each set of boundary conditions – except stainless steel specimens with CFCF boundary conditions, which underwent only 100 experiments. For aluminum specimens shown in Table 2, the percent difference of the measured buckling loads from the benchmarks varies from -5.95% to 4.10% . However, the averages of the discrepancies for specimens with the same boundary conditions, shown at the bottom of the table, are less than $\pm 2\%$. It is also observed that the average percent difference is independent of the size, thickness and boundary condition of the specimen. In general, the buckling load of an aluminum specimen obtained from VCT matches the numerical solution very well. On the other hand, measured buckling loads of stainless steel plates do not agree as well with the numerical ones. As shown in Table 3, the percent discrepancies of the measured buckling loads of CCCF and CFCF specimens are comparable to those of aluminum plates. The average differences of buckling load for both boundary conditions are less than 1%. However, the average difference of 11.41% for CCCC specimens is fairly high compared with other experiments. It is also evident that the measured buckling load of a thicker plate deviates from the expected solution more than does that of a thinner one. Specifically, the percent differences of the thicker plates (specimens #2, 4 and 6) vary from 13.45% to 16.15% – a greater variance than those of the thinner plates (specimens #1, 3 and 5) which are all less than 10%.

4.2.1 Imperfection of boundary conditions

From the experimental results of CCCC stainless steel specimens, it is speculated that the boundary condition of those specimens significantly deviates from the theoretical one. For a clamped support, the specimen should be fixed with zero out-of-plane displacement and zero slope on the boundary. After careful consideration, it was hypothesized that the supports on the unloaded edges were liable to be the cause of the observed imperfection. These supports are restrained by two support holders which are clamped on the guided columns, as shown in Fig. 5. Ideally, the support holder will not rotate around the guided column, so that the specimen remains tightly secured by the clamped supports. However, if the bending moment on a specimen's edge is sufficiently high, the support holder could be rotated by the reaction moment, resulting in a movement of the support in the out-of-plane direction. As a result, an imperfection of the clamped boundary condition could be observed by monitoring the movement of the support bar on the unloaded edge. An additional measurement was conducted on both aluminum and stainless steel specimens to investigate the perfection of the clamped boundary condition. Specimens #1 and 2 were mounted on the test frame and loaded with tensile loading, similar to that of the vibration test to determine natural frequencies. A dial indicator was placed in the middle of a clamped support to monitor the motion of the support after the specimen was loaded with tensile loading. A plot of the displacement in the out-of-plane direction of the support, versus applied tension, is presented in Fig. 11. Ideally this displacement should not exist at any load level. However, this displacement can be detected if: (a) the specimen

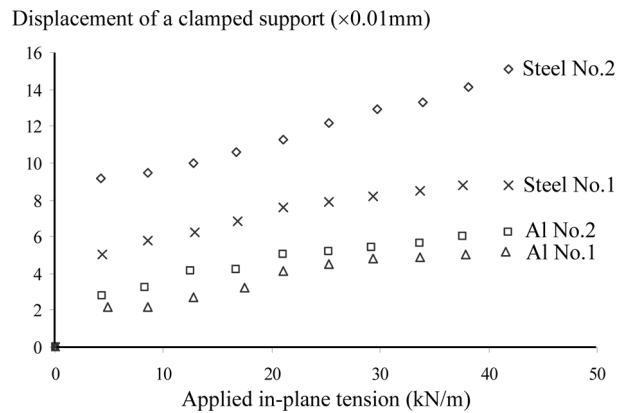


Fig. 11 Plot of support displacement vs. in-plane tension of CCCC specimens

is not perfectly flat; or (b) the tensile load is not uniformly applied. It should also be noted that the nominal sizes of specimens #1 and 2 are identical, but that specimen #1 is thinner than specimen #2. It can clearly be seen that the displacements of the supports on the stainless steel plates are considerably greater than those on the aluminum plates. Furthermore, the measured displacements of thinner plates are less than those of thicker plates. This out-of-plane displacement of the support indicates the imperfection of that support. So, based on the test frame used in this study, it can be concluded that aluminum specimens are better supported by a clamped boundary condition on the unloaded edges than are the stainless steel specimens. Similarly, a clamped support on a thinner specimen is closer to an ideal boundary condition than that on a thicker specimen. Although all specimens were clamped with the same supports and comparable clamping force, they were probably not subjected to similar boundary conditions because of differences in the plates' bending stiffness. The bending stiffness of a stainless steel plate is greater than that of an aluminum plate, as is a thicker plate compared with a thinner plate. Because of the imperfections of plates and loading conditions, such as preexisting curvatures and uniformity of tensile loading, specimens have a tendency to move in the out-of-plane direction. With an ideal boundary condition, all of this motion will be suppressed by the clamped support. It is confirmed by additional measurement that the support cannot completely restrain the specimen, as shown in Fig. 11. Specimens with lower stiffness, i.e., aluminum plates and thinner plates, are better supported with a clamped boundary condition. Thus, the buckling loads of CCCC stainless steel specimens are not easily predicted compared with those of other specimens, because the boundary conditions of these specimens significantly diverge from an ideal boundary condition. In addition, the supports on thinner specimens (#1, 3 and 5) resemble a near-ideal boundary condition more closely than do those of thicker ones. This assertion is supported by the plot in Fig. 11, and explains the obtained percentage differences of the CCCC stainless steel specimens.

Any imperfection of the clamped supports, i.e., rotation of the support holder, will be encountered only on the unloaded edges. The clamped supports on the loaded edges are mounted on crossheads #2 and #3, which are only allowed to move along two guided columns. With the described arrangement, both crossheads cannot be rotated as long as the guided column remains straight; so the supports on these edges closely resemble an ideal clamped boundary condition. Therefore, this setup of the boundary conditions of the CFCF specimens allowed accurate identification of the

buckling loads of CFCF specimens, using VCT. For CCCF boundary conditions, even though one of the unloaded edges was supported with a clamped boundary condition, the experimental buckling loads from VCT still matched the numerical solutions very well. The unloaded edges on the CCCF specimens are clamped on one side and free on the other side. The free edges of these specimens are allowed to deform or bend; consequently, the bending moment on the other unloaded edges is probably not high enough to nullify a clamped boundary condition.

The experimental results demonstrate that the measured buckling loads of all of the CCCC stainless steel specimens are higher than the theoretical ones: i.e., the percent differences are positive. This observation is contradicted by the fact that the specimens were not perfectly clamped, so their buckling loads should have been lower than those of the numerical solutions. However, this contradiction is rational because the measured buckling load is obtained from the measured vibration data. Because of the divergent boundary conditions, the specimens are not perfectly restrained; so their boundary conditions lie somewhere in between simple support and clamped support. Thus, the measured natural frequencies of the specimens subjected to tensile load are lower than those of the perfectly clamped specimens. The degree of divergence of the boundary conditions is greater when the specimen is loaded with higher in-plane load. As a result, the slope of the trend line of ω^{*2} vs. N_x is lower than expected, and the intersection of the trend line with the N_x -axis is farther away from the origin than it should be. Therefore the buckling load obtained from VCT using vibration data in the tensile loading region is higher than that found in theory.

In conclusion, specimens used in this study were either supported with a clamped support or had a free boundary condition. The clamped boundary conditions on the loaded edges, as well as the free boundary conditions on the unloaded edges, were appropriately set up. Imperfection of the clamped boundary condition on the unloaded edge was reduced if the boundary condition on the other edge was a free boundary condition. The imperfection of the support was also minimized on the aluminum specimens because of the plates' lower degree of stiffness. Only CCCC stainless steel plates were not well supported by the intended clamped boundary condition. This observation clarifies the fact that the VCT-measured buckling loads of these specimens diverge from the numerical solutions. Buckling loads of other sets of specimens are accurately indicated using the proposed technique.

4.2.2 Deviation of the buckling load

The average percent differences of the measured buckling loads from the numerical solutions are very low for most of the experiments with properly prepared boundary conditions. However the standard deviations of the percent differences for each group of specimens are, on the other hand, fairly high. The standard deviation for specimens with the same material and boundary condition is shown in the last rows of Table 2 and 3. Unlike the average percent discrepancies, the standard deviations are not significantly different. For CCCC and CCCF specimens, the standard deviations of the percent difference varied from 4% to 6.5% for both materials. The standard deviations of CFCF specimens were 3.38% and 3.76% for aluminum and stainless steel plates, respectively. These deviations are somewhat less than those of the specimens with CCCC and CCCF boundary conditions. The standard deviation of the percent difference indicates the precision or repeatability of the measurements. In the experiment, to obtain a buckling load a specimen was clamped by tightening machine screws, and then tested for natural frequencies under an increasing tensile loading. The supports on the specimen were then loosened and retightened again for the next experiment. Hence, the boundary conditions of the specimens for each measurement are not

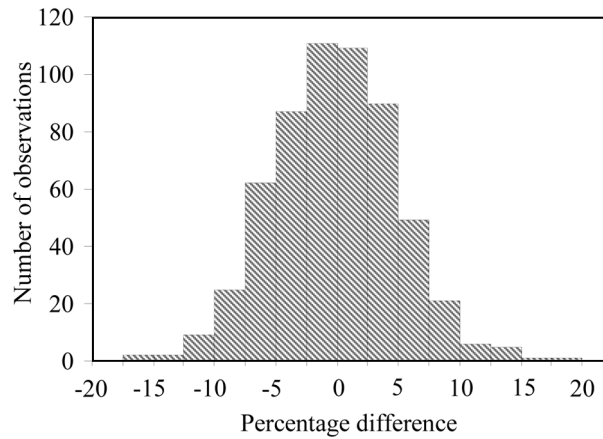


Fig. 12 Histogram of the percentage difference between measured and predicted buckling loads of the experiment (not including CCCC of stainless steel)

identical. Additional tests were conducted by repeating the experiment without loosening the machine screws (i.e., the same boundary conditions were maintained). The resulting measured buckling loads were not significantly different. Therefore, the measured buckling load of one experiment deviates from those of other experiments because of the nonidentical boundary condition between each experiment. It is also noteworthy that the boundary condition on the unloaded edges of a CFCF specimen is free, or unsupported. So the boundary condition on these edges is identical for all experiments. Accordingly, the boundary conditions of CFCF specimens deviate less, from experiment to experiment, than do those of specimens with other boundary conditions. As a result, the standard deviations of the percent differences of CFCF specimens are markedly less than those of specimens with other boundary conditions.

The distribution of the percent differences in the experiments with properly-set boundary conditions is presented as a histogram, shown in Fig. 12. The experimental results of CCCC stainless steel plates are not included in the plot because of their ill-defined boundary conditions. There are a total of 580 comparisons between the measured and numerical buckling loads. It can be seen that the histogram resembles a symmetrical bell curve, with the tip of the curve at around 0%. The average percent difference from 580 comparisons is -0.18% , with a standard deviation of 5.05% . A total of 397 comparisons, or approximately 68%, have a percentage difference between measured and numerical buckling loads within $\pm 5\%$.

In conclusion, the accuracy of using VCT with vibration data in the tensile loading region to identify the buckling load of plates is very well demonstrated. The precision or repeatability of the experimental technique is quite acceptable, given the fact that the boundary conditions of the specimens in this study were not precisely identical. In practice, the precision of using VCT can be maximized if the boundary conditions of the specimens are suitably arranged. The advantage of using VCT is that the technique is applicable for specimens with any boundary conditions. As long as the specimen in the vibration test is supported in the same manner as in the buckling problem, the buckling load obtained from VCT should be accurate and precise, regardless of the boundary conditions of the specimen.

5. Conclusions

The relationship between the natural frequency and the buckling load of a rectangular thin plate is addressed in this study. It is shown that the square of the natural frequency of a loaded plate varies linearly with the in-plane load. By comparing the governing equations of both problems, the natural frequency of the plate decreases to zero when the applied in-plane load approaches the buckling load of the plate. The derived relationship can be utilized as a technique to identify the buckling load and buckling mode of the structure. Due to a premature curvature which usually develops before buckling, the use of vibration data in the tensile loading range, where the premature curvature is negligible, is proposed in this study. To verify the accuracy of the technique, the experiment was performed on a test frame in which the specimens were loaded and tested for natural frequencies. Both aluminum and stainless steel specimens with CCCC, CCCF and CFCF boundary conditions were included. The measured vibration data was plotted against the in-plane load to determine the buckling load and buckling mode. The square of the measured natural frequency varies linearly with the applied load, as expected. The experimental results show that all buckling modes obtained from VCT agree very well with the numerical solutions, while most of the measured buckling loads also conform to the numerical solutions. The buckling loads of CCCC stainless steel specimens were not clearly indicated using the proposed technique. The imperfection of the boundary conditions in this group of specimens is believed to be the primary factor in the high percentage difference between the measured and numerical buckling loads. If the experiments using stainless steel specimens with CCCC boundary conditions are excluded, the average percent difference between measured buckling loads and numerical solutions is -0.18%, with a standard deviation of 5.05%. The obtained percent difference resembles a normal, bell-shaped distribution. The standard deviation is fairly high because of the variation in boundary conditions from one experiment to another.

In conclusion, the experimental study demonstrates the accuracy and reliability of using vibration data in the tensile loading range to determine buckling load. Boundary conditions of the specimen have a considerable effect on the precision of the measured buckling load. The proposed technique of identifying the buckling load of a plate has an advantage over static methods, in that this method does not require human judgment to draw lines in the pre- and post-buckling regions. However, the boundary conditions of the specimen must be carefully set in order to obtain an accurate and precise measurement. The measured natural frequency of the specimen is sensitive to the boundary conditions and, hence, is a critical parameter in applying VCT to the plate buckling problem.

Acknowledgements

This research is supported by the Commission on Higher Education and the Thailand Research Fund under project grant #RMU4880021.

References

- Avitabile, P. (2001), "Experimental modal analysis: a simple non-mathematical presentation", *J. Sound Vib.*, **35**(1), 20-31.

- Aydogdu, M. and Timarci, T. (2003), "Vibration analysis of cross-ply laminated square plates with general boundary conditions", *Compos. Sci. Tech.*, **63**(7), 1061-1070.
- Chai, G.B., Banks, W.M. and Rhodes, J. (1991), "An experimental study on laminated panels in compression", *Compos. Struct.*, **19**(1), 67-87.
- Chailleux, A., Hans, Y. and Verchery, G. (1975), "Experimental study of the buckling of laminated composite columns and plates", *Int. J. Mech. Sci.*, **17**, 489-498.
- Ding, Z. (1996), "Natural frequencies of rectangular plates using a set of static beam functions in Rayleigh-Ritz method", *J. Sound Vib.*, **189**(1), 81-87.
- Go, C.G., Lin, Y.S. and Khor, E.H. (1997), "Experimental determination of the buckling load of a straight structural member by using dynamic parameters", *J. Sound Vib.*, **205**(3), 257-264.
- Go, C.G. and Liou, C.D. (2000), "Experimental determination of the buckling load of a flat plate by the use of dynamic parameters", *Struct. Eng. Mech.*, **9**(5), 483-490.
- Lee, J.M., Chung, J.H. and Chung, T.Y. (1997), "Free vibration analysis of symmetrically laminated composite rectangular plates", *J. Sound Vib.*, **199**(1), 71-85.
- Lurie, H. and Monica, S. (1952), "Lateral vibrations as related to structural stability", *J. Appl. Mech.*, **19**, 195-204.
- Ni, Q.Q., Xie, J. and Iwamoto, M. (2005), "Buckling analysis of laminated composite plates with arbitrary edge supports", *Compos. Struct.*, **69**(2), 209-217.
- Rajalingham, C., Bhat, R.B. and Xistris, G.D. (1996), "Vibration of rectangular plates using plate characteristic functions as shape functions in the Rayleigh-Ritz method", *J. Sound Vib.*, **193**(2), 497-509.
- Segall, A. and Springer, G.S. (1986), "A dynamic method for measuring the critical loads of elastic flat plates", *Exp. Mech.*, **26**(4), 354-359.
- Singer, J., Arbocz, J. and Weller, T. (1992), *Buckling Experiments: Experimental Methods in Buckling of Thin-walled Structures*, Vol. 1, John Wiley & Sons, Chichester, UK.
- Singhatanadgid, P. and Sukajit, P. (2008), "Determination of buckling load of rectangular plates using measured vibration data", *Proceedings of the International Conference on Experimental Mechanics*, Nanjing, China, November.
- Souza, M.A. and Assaid, L.M.B. (1991), "A new technique for the prediction of buckling loads from nondestructive vibration tests", *Exp. Mech.*, **31**(2), 93-97.
- Timarci, T. and Aydogdu, M. (2005), "Buckling of symmetric cross-ply square plates with various boundary conditions", *Compos. Struct.*, **68**(4), 381-389.
- Tuttle, M., Singhatanadgid, P. and Hinds, G. (1999), "Buckling of composite panels subjected to biaxial loading", *Exp. Mech.*, **39**(3), 191-201.
- Wang, G., Wereley, N.M. and Chang, D.C. (2005), "Analysis of bending vibration of rectangular plates using two-dimensional plate modes", *J. Aircraft*, **42**(2), 542-550.